Advances in Applied Mathematics and Mechanics
Adv. Appl. Math. Mech., Vol. **3**, No. 3, pp. 310-326

DOI: 10.4208/aamm.10-10s2-04
June 2011

Heat Transfer, Knock Modeling and Cyclic Variability in a "Downsized" Spark-Ignition Turbocharged Engine

Fabio Bozza[1,*], Daniela Siano[2] and Michela Costa[2]

[1] *Università di Napoli "Federico II", DIME, Via Claudio 21, 80125 Napoli, Italy*
[2] *Istituto Motori-CNR, Viale Marconi 8, 80125 Napoli, Italy*

Received 14 January 2010; Accepted (in revised version) 18 August 2010

Available online 28 February 2011

Abstract. In the present paper a combined procedure for the quasi-dimensional modelling of heat transfer, combustion and knock phenomena in a "downsized" Spark Ignition two-cylinder turbocharged engine is presented. The procedure is extended to also include the effects consequent the Cyclic Variability. Heat transfer is modelled by means of a Finite Elements model. Combustion simulation is based on a fractal description of the flame front area. Cyclic Variability (CV) is characterized through the introduction of a random variation on a number of parameters controlling the rate of heat release (air/fuel ratio, initial flame kernel duration and radius, laminar flame speed, turbulence intensity). The intensity of the random variation is specified in order to realize a Coefficient Of Variation (COV) of the Indicated Mean Effective Pressure (IMEP) similar to the one measured during an experimental campaign. Moreover, the relative importance of the various concurring effects is established on the overall COV. A kinetic scheme is then solved within the unburned gas zone, characterized by different thermodynamic conditions occurring cycle-by-cycle. In this way, an optimal choice of the "knock-limited" spark advance is effected and compared with experimental data. Finally, the CV effects on the occurrence of individual knocking cycles are assessed and discussed.

AMS subject classifications: 76N15, 62P30, 80A20, 80A25.

Key words: Finite elements in heat transfer, internal combustion engines modelling, cyclic variability, knock.

1 Introduction

The phenomenon of Cyclic Variability (CV) in internal combustion engines, a known issue since the end of the 19th century, is nowadays particularly relevant in the autom-

*Corresponding author.
URL: `http://boxxa.dime.unina.it/~fbozza`
Email: fabio.bozza@unina.it (F. Bozza), d.siano@im.cnr.it (D. Siano), m.costa@im.cnr.it (M. Costa)

otive research, due to the measures that are being adopted to fulfil more and more stringent legislative constraints about the pollutants emissions at the exhaust. As an example, there is a trend to a convergence between the Spark Ignition (SI) engine and the Compression Ignition (CI) engine in operating under lean mixture conditions and with high percentages of Exhaust Gas Recirculation (EGR) to increase the fuel economy and minimize the NO emissions. In these situations CV occurs with a high frequency and actually limits the potential benefits which can be derived from these operating modes.

During normal engine operation, cycle-by-cycle fluctuations are expected in the rate of heat release, hence in the amount of useful work done by a single combustion event, in the fuel consumption and the exhaust emissions. Due to its unpredictable and stochastic character, CV poses several problems to the development of optimal engine control systems [1, 2] and limits the vehicle drivability. CV is a consequence of the early flame development conditions, that deeply influence the subsequent combustion phase [3]. The flame kernel formation depends on local mixture composition and thermo-fluid-dynamic conditions at the spark plug location. These are affected by various factors, as the spatial and temporal fluctuations of the turbulent flow field inside the cylinder, the not perfectly homogeneous nature of the mixture at the spark time and the continuous adjustment of the gasoline injected mass and possible EGR amount, actuated by the engine closed-loop control system. This last, on the other hand, suffers from time delays and noise disturbances of the processed signals. Although the complex interaction of the above phenomena is not yet fully understood, it is widely recognized that CV is particularly felt at cold starting, idling, low load, and lean or highly diluted mixture operation [4], where the burning velocity is slow and the flame development is difficult. In this sense CV also limits the engine tolerance to EGR, and penalizes the fuel consumption of Variable Valve Timing (VVT) equipped engines [5], where internal EGR is realized to the aim of virtually reducing the engine displacement at low load.

Moreover, recently, a tendency is being consolidated to produce low displacement turbocharged SI engines. This design philosophy, known as "engine downsizing", allows to reduce mechanical and pumping losses at low load as a consequence of the higher operating Brake Mean Effective Pressure (BMEP). The turbocharger permits to restore the maximum power output of larger displacement engines. Additional advantages are a higher low-speed torque and a better drivability and fun-to-drive. Of course, at high loads, the spark-advance and heat transfer phenomena through the cylinder walls must be carefully controlled to avoid the knock occurrence. Even small differences of the unburned gas temperature, related to variations in the heat transfer rate and the spark-advance setting, non-linearly affect the knocking onset. For this reason, the knowledge of the heat transfer details is crucial to carefully compute the so-called "knock-limited spark timing", being a key point for the reduction of the fuel consumption drop at high loads. From this point of view, the effects resulting from CV play a fundamental role. CV mainly causes fluctuations in the heat released by the combustion process and heat losses through the walls, turning in fluctuations

in the unburned gas temperature. In addition, since the spark timing is usually set for the "average" operating cycle, faster-than-average burning cycles are most likely to knock. The optimal "knock-limited" spark advance must therefore be chosen by taking into account both the heat transfer regime and the CV.

In the present paper, a quasi-dimensional combustion model [6, 7] is extended to characterize the CV of a turbocharged SI engine. Heat transfer is simulated by means of a procedure based on a Finite Elements (FE) model of the combustion chamber. Inputs to the FE model include combustion chamber geometry, coolant and oil temperatures. The relevant convective heat transfer coefficients on the coolant water side are adjusted as a function of the engine regime. CV is computed by introducing proper random variations on a number of parameters that affect the heat release rate (air/fuel ratio, initial flame kernel duration and radius, laminar flame speed, turbulence intensity). The combustion model, utilizing a deeply validated approach, is based on a fractal schematization of the flame front surface. The combustion model is included within a 1D simulation code and is coupled to a chemical kinetic solver (CHEMKIN), for the estimation of the knocking onset. The latter is carried out for each individual engine cycle, through the solution of a kinetic scheme inside the "end-gas" unburned zone. This allows to estimate a statistical distribution of a proper knocking index, able to identify the presence of knocking cycles, even in the absence of knocking on the average cycle.

The intensity of the random variation is specified in order to realize an Indicated Mean Effective Pressure (IMEP) Coefficient Of Variation (COV) similar to the one observed during an experimental campaign conducted at the test bench. Moreover, the relative importance of the various concurring effects (by changing each of them as separate from each other) is assessed. The COV of the IMEP and of the numerical knock indicator are finally compared and discussed.

2 Engine model and heat transfer

A quasi-dimensional turbulent combustion model has been developed since many years at the University of Naples-DIME, based on the "wrinkled-flamelet" combustion regime. It is based on a two-zone approach and includes a fractal schematization of the flame front surface. Main feature of the model is the possibility to relate the mixture burning rate to the turbulence flow characteristics inside the combustion chamber. In particular, the fractal dimension of the flame and its wrinkling scales are defined as a function of the mean turbulence intensity inside the combustion chamber. To this end, a modified zero-dimensional turbulence model (k-K model [8]) is coupled to the fractal combustion model. Detailed 3D analyses carried out in [9] are utilized to accurately "tune" the 0D turbulence model for a turbocharged SI engine quite different from the one under investigation. Both the combustion and the turbulence sub-models are implemented in the 1D GT-Power code for the simulation of the whole propulsion system, from the intake mouth to the exhaust tailpipe [10]. Despite

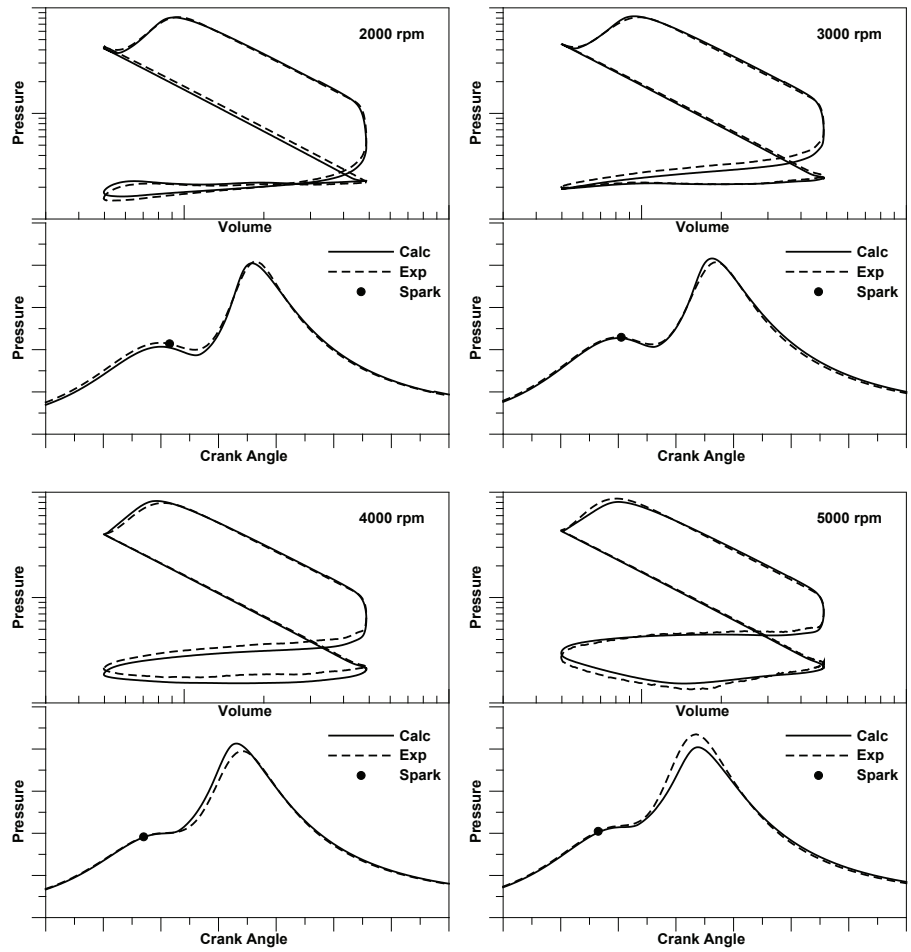

Figure 1: Comparisons between numerically computed and experimentally measured average pressure cycles at different engine speeds.

differences in the engine architecture, tuning constants of both the turbulence and the combustion model assume the same values reported in [9], and are left unchanged in each operating condition.

Computed pressure cycles for the two-cylinder turbocharged engine here considered are compared in Fig. 1 with experimental data collected at different speeds under Wide Open Throttle (WOT) conditions. Experimental data are ensemble averaged over 94 consecutive cycles. In order to better appreciate the quality of the numerical results, both the combustion period and the whole engine cycle are reported in a $p-\vartheta$ and $\log(p)-\log(V)$ plane, respectively. At each engine speed, the spark timing is set as the maximum allowable advance for a knock-free operation on the average cycle. The above value is experimentally derived basing on an accelerometer signal, located on the engine block. A very retarded combustion process is established especially at low speed, producing the presence of two pressure peaks. The angular

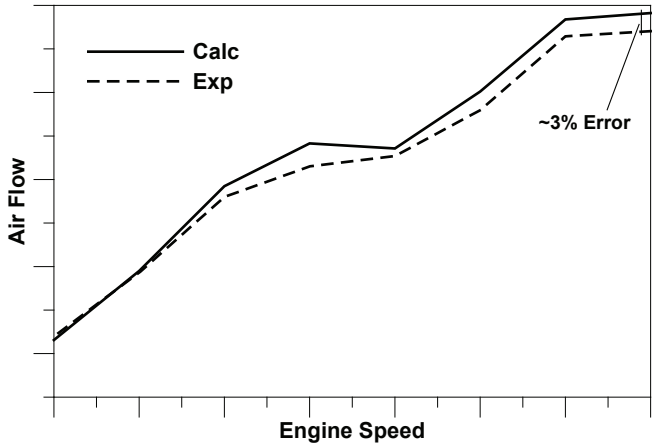

Figure 2: Comparison between numerically computed and experimentally measured air flow rates at the intake as a function of the engine speed.

delay between the spark and the time of the first pressure rise is well reproduced by the model. Moreover, the satisfactory agreement along the compression stroke and during the pumping phase suggests that a good matching with the turbocharger and an adequate simulation of the unsteady flow in the intake and exhaust systems is also obtained. The latter consideration is also proved by the comparison on the intake air flow rate, shown in Fig. 2.

The accuracy of the model also depends on the inclusion of a detailed heat transfer model that allows the prediction of the cylinder wall surface temperatures in various combustion chamber zones. The calculation of the wall temperatures is based on a FE model of the head, valves, cylinder liner, and piston. This model, included in the 1D simulation code GT-Power [10], is generated from the supplied geometric characteristics and some general assumptions regarding the combustion chamber geometry, schematised in Fig. 3. The conductive heat transfer coefficient is defined based on the material properties and dimension. The convective heat transfer coefficients on the coolant water side and oil side are adjusted as a function of the engine regime: starting from the values relevant to the lower considered engine speed, they are adjusted as growing with the Reynolds number to the power 0.85, being the Reynolds number assumed as scaling proportionally with the engine speed. An example of the heat transfer rates for the engine speed of 5500rpm, full load operation, is reported in Fig. 3. For the same operating condition, Fig. 4 represents the temperature distribution predicted by the model on the cylinder head. The temperatures of particular macro-zones, representing selected groups of elements of the FE mesh, are displayed as a function of the engine speed in Fig. 5. The predicted temperature levels and the overall trends seem in good agreement with expected literature values.

An accurate prediction of the unburned gas temperature and pressure is hence available, that allows coupling the thermo-dynamic engine model to the kinetic solver for knocking calculations, described in the following section.

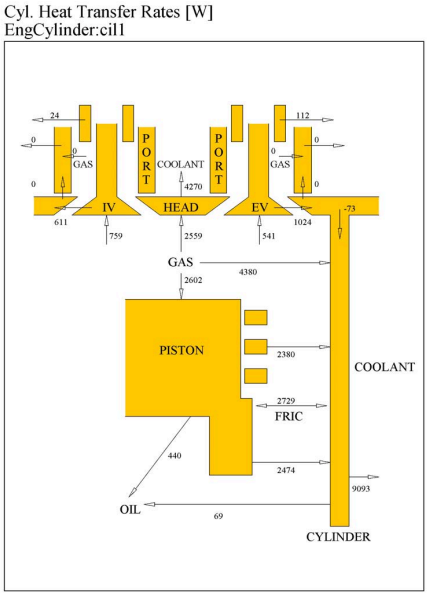

Figure 3: Schematization and heat transfer rates (W) of the combustion chamber. Engine speed: 5500rpm, full load operation.

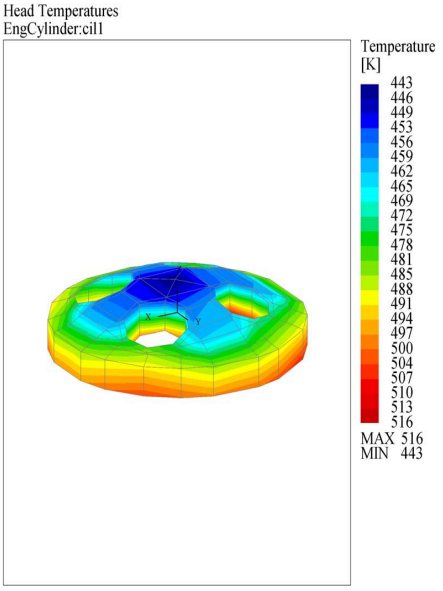

Figure 4: Temperature distribution on the cylinder head. Engine speed: 5500rpm, full load operation.

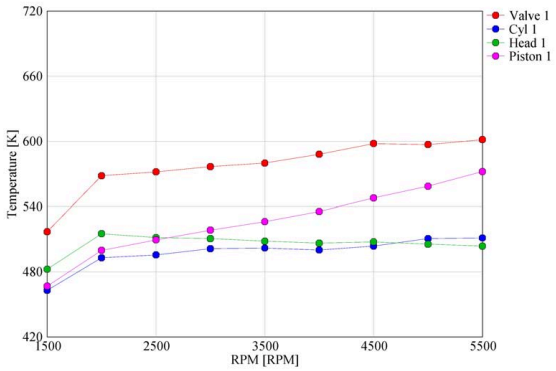

Figure 5: Computed wall temperatures in the combustion chamber.

3 Knock model

Under the hypothesis of the presence of N_{spec} chemical species in the unburned gases, a rearrangement of the energy equation in the unburned zone (subscript u) during the closed valve period leads to the following relationships:

$$\frac{dT_u}{dt} = \left(V_u \frac{dp}{dt} + \frac{dQ_{chem}}{dt} - \frac{dQ_w}{dt}\right)(m_u c_{pu})^{-1}, \tag{3.1a}$$

$$\frac{dQ_{chem}}{dt} = -m_u \sum_{1}^{N_{spec}} e_i \frac{dx_i}{dt}. \tag{3.1b}$$

In the above equations, p, T, V, m, c_p, e, respectively represent the pressure, temperature, volume, mass, specific heat coefficient and specific internal energy of the unburned gases. The variation in composition (dx_i/dt) of the i^{th} specie in Eq. (3.1b) is computed through the solution of a reaction kinetic scheme in the unburned zone. As a consequence, a certain amount of heat is released (dQ_{chem}/dt), denoting the occurrence of the autoignition phenomenon. Two knock indicators can be consequently defined:

$$Q_{ub} = \int \frac{dQ_{chem}}{dt} dt, \qquad x_{Qub} = \frac{Q_{ub}}{m_f LHV}. \tag{3.2}$$

The first term (Q_{ub}) represents the total heat released in the unburned gases, while the second (x_{Qub}) is the same quantity normalized with respect to the overall chemical heat made available from the injected fuel. Results presented in the following refer to a reduced kinetic mechanism developed for the simulation of the combustion of mixtures of iso-octane and n-hepthane, developed by Tanaka and Keck [11, 12] and including 5 elements, 32 species and 55 reactions. The mechanism handles both low and high temperature reactions and is tuned to reproduce the end-gas conditions in a SI engine [13].

In order to predict the values of the spark advance that guarantees a knock free operation, a virtual knock-sensor and a PID controller are included in the 1D simulation code. At the end of each engine cycle, the sensor "measures" the instantaneous value of the Q_{ub} parameter and the PID controller updates the spark timing until a threshold value is reached. This is assumed at a very low value, namely 20J, corresponding, for the selected engine and analyzed WOT operating conditions, to an average level of about 0.6% of the total heat released ($m_f LHV$). In this way the set level defines how much "light knocking" is acceptable. It must be pointed out that the above threshold can be really considered as a sort of "tuning constant" of the model. It simply scales with the unit displacement, even if different fuels or a different experimental determination of the knocking onset may require an adjustment of the scaled level. As a matter of fact, it is important to stress that a unique value of this parameter allows predicting the knock-limited spark advance at different operating conditions.

Fig. 6 shows an example of the spark advance time history, starting from an initial value of 40° Before the Top Dead Centre (BTDC), and the related values of the Q_{ub} knock indicator, at 4000rpm. At the end of the simulation, the set value of the knock indicator is reached and the corresponding knock-limited spark advance is obtained. The PID controller parameters are properly tuned to guarantee that no deviation between the set point and the final Q_{ub} level remains for all the investigated cases. Results very similar to those displayed in Fig. 6 are achieved at each engine speed.

Fig. 7 reports the comparison between numerically predicted and experimentally assessed knock-limited spark timings, at different engine regimes. The overall trend is well predicted and the agreement seems satisfactory, also considering some difficulties in the experimental determination of the incipient knocking conditions. As expected, lower engine speeds exhibit the most critical conditions and require a very reduced or negative spark advance.

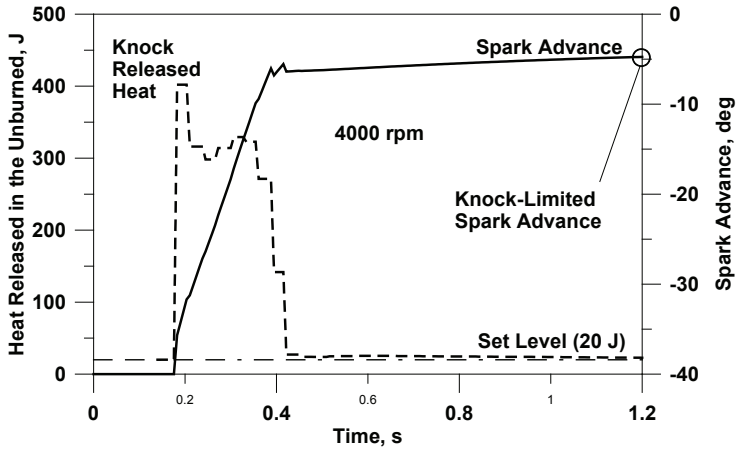

Figure 6: Time-history of the knock-limited spark timing.

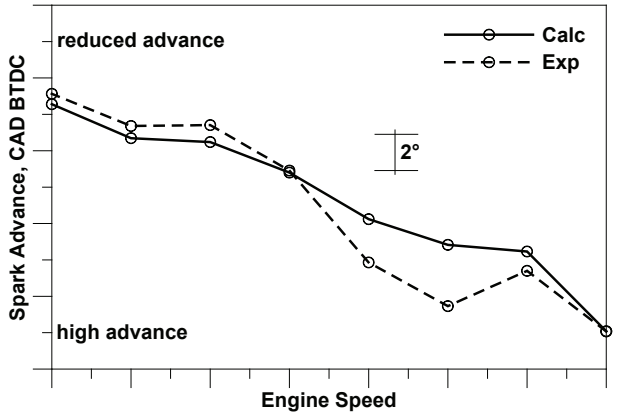

Figure 7: Comparison between the numerically computed and the experimentally evaluated knock-limited spark advances.

It is to be noticed that although the initial spark timing is set far away ($-40°$) from the experimental level, the final error is in many cases lower than $1°$ crank angle. The maximum error is slightly higher than $2°$. Unfortunately, the calculation of about 150 consecutive cycles in each operating point is really required to reach the PID controller convergence. The computation of the spark advance profile in Fig. 7, therefore, needs about 4 hours on a common PC. The proposed methodology seems, in any case, a good compromise solution between accuracy and reduced computational time and allows to efficiently provide a very good "off-line" estimation of the knock-limited spark advance, to be possibly refined on the test-bench.

The so far described analysis is carried out with reference to average pressure cycles. For this reason, no information can be derived by the model on the presence of individual knocking cycles, related to CV phenomena. In the following, a simple cycle-to-cycle variation model is described, with the aim of deriving a statistical distribution of a knock indicator, for each engine regime.

4 Cyclic variability

To the aim of characterizing the CV phenomenon, a random perturbation is introduced in the combustion model on a number of parameters usually considered as the most important controlling factors [2], namely:

1. flame kernel duration;
2. flame kernel radius;
3. air/fuel ratio;
4. laminar flame speed;
5. turbulence intensity.

In the quasi-dimensional combustion model here employed, flame kernel duration and radius affect the ignition delay time. The other parameters (A/F ratio, laminar flame speed and turbulence intensity) influence the turbulent flame speed and the burning rate. At the beginning of each engine cycle, each parameter in the above list (P_i) is randomly perturbed with respect to its average value ($P_{i,av}$), within a prescribed x_{band} range, as:

$$P_i = P_{i,av} * rnd(1 \pm x_{band}), \qquad i = 1,5. \tag{4.1}$$

The superimposition of these perturbations non-linearly affects the rate of heat release and the pressure cycle. Consequently, it determines a cycle-by-cycle IMEP variation. The range of random variation (x_{band}) is expected to change with the engine operating conditions. Moreover, a different variability range may actually occur on each controlling parameter, P_i. For the sake of simplicity, indeed, a unique x_{band} range is here specified. CV is quantified by means of the Coefficient Of Variation (COV) of the IMEP, defined as:

$$COV_{IMEP} = \frac{\sigma_{IMEP}}{IMEP_{av}} * 100. \tag{4.2}$$

σ_{IMEP} being the IMEP standard deviation, and $IMEP_{av}$ the related average level. The above parameter is experimentally estimated, at each engine speed, through the measurement of 94 consecutive pressure cycles. Numerical data refer to 490 cycles, apart from those required to get a stationary engine-turbocharger matching. COV_{IMEP} values plotted in Fig. 8 are always well below 5%, usually considered as the upper acceptable limit under the point of view of engine drivability. They do not reveal any particular relation with the engine speed or other typical engine operating parameters, and only exhibit a random character. For this reason, a good agreement between experimental and computed COV data can only be found if the x_{band} parameter in Eq. (4.1) is adjusted at each operating condition. "Tuned" x_{band} values are reported in the same Fig. 8 at each engine speed. They are very well correlated to COV itself, as displayed in Fig. 9.

In order to establish the relative importance of each of the previously listed five parameters, an additional investigation is realized by activating the related random

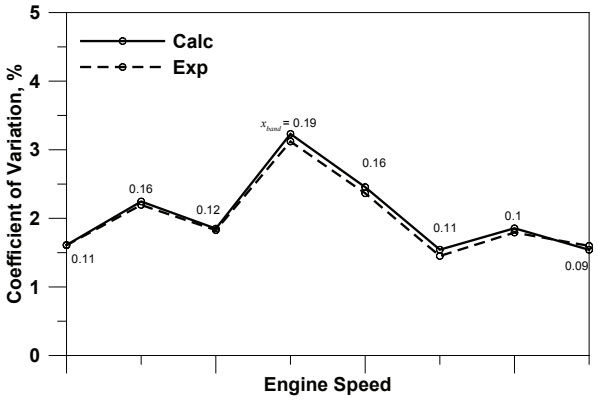

Figure 8: Computed and experimental IMEP COV profiles.

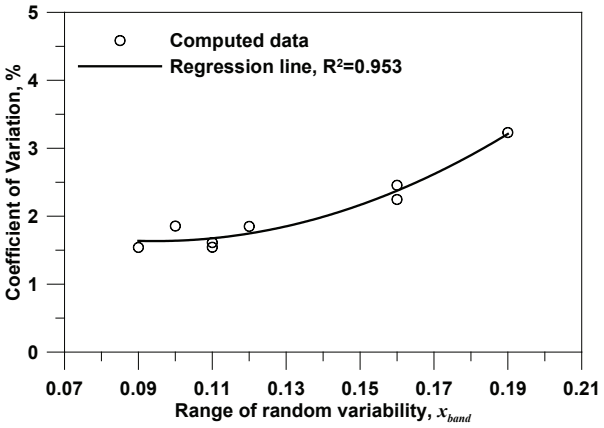

Figure 9: Correlation between COV and x_{band}.

perturbations once at a time, in a single operating condition and with the same x_{band} value. Results of this analysis are reported in Fig. 10. This shows that both the flame kernel duration and radius only exert a limited influence on the overall COV, while a greater and similar importance is played by the laminar flame speed and the turbulence intensity. These results agree with some theoretical findings reported in [19]. However, differences in the single variability ranges or analyses in different operating conditions may alter the importance weights shown in Fig. 10. Moreover, the non-linear dependence of the burning rate on the five considered parameters implies that the overall COV is not linearly linked to the single COV_i. A complex superimposition of each single effect really contributes to the overall variability. For this reason, in the following, variations of all the parameters are considered.

Figs. 11 and 12 report the experimental and computed pressure fluctuations at two different engine regimes. Computed data refer to the tuned values of the x_{band} parameter, reported in Fig. 9. Experiments and computations exhibit a similar qualitative behavior in terms of peak pressure and angle of peak pressure fluctuations. A

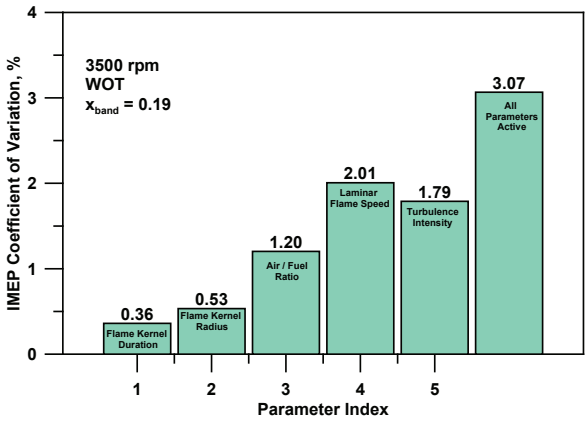

Figure 10: Coefficient of variation of the IMEP as a function of variations of the controlling factors for the combustion model.

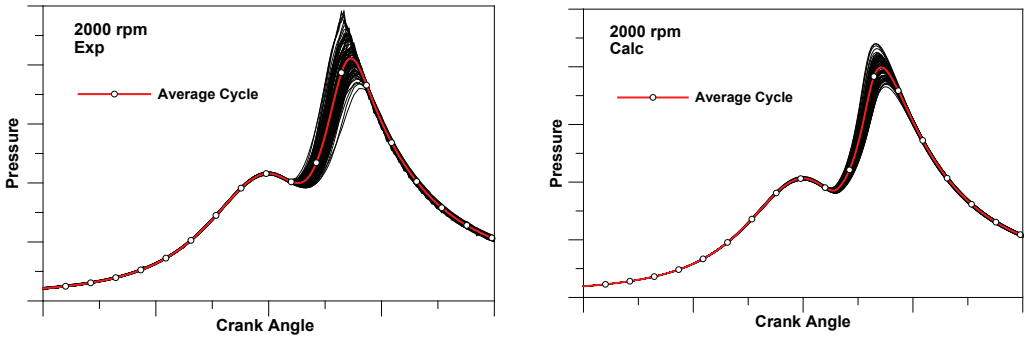

Figure 11: In-cylinder pressure fluctuations at 2000rpm.

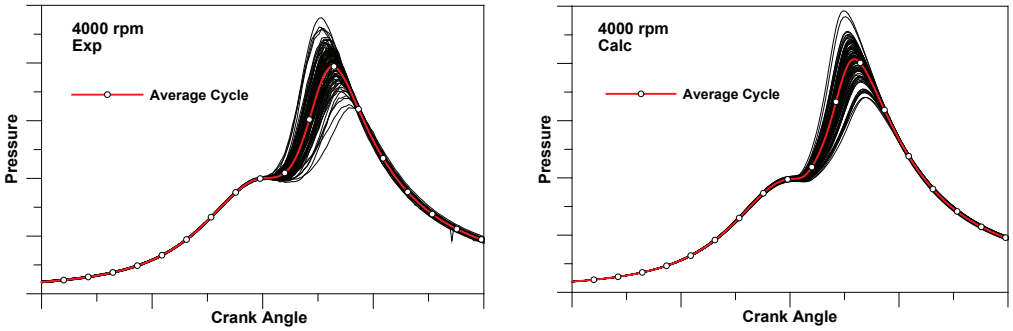

Figure 12: In-cylinder pressure fluctuations at 4000rpm.

more quantitative analysis is reported in Figs. 13 and 14, displaying the experimental and numerical distributions of the "normalized" IMEP ($IMEP/IMEP_{av}$) for the same regimes of Figs. 11 and 12, respectively. A good agreement of the Gaussian Distribution fit is obtained, also considering the reduced amount of the experimental pressure cycles population (94 cycles).

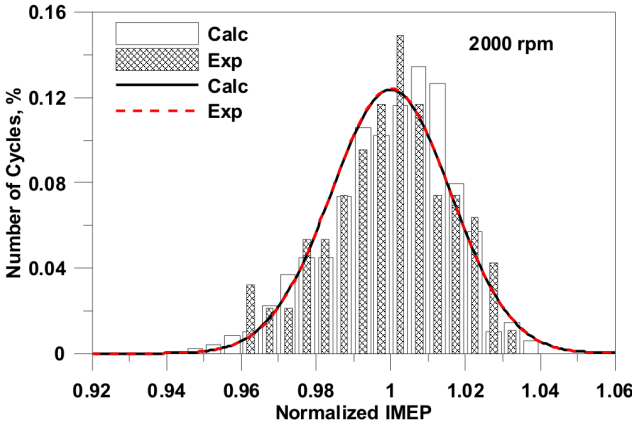

Figure 13: Computed and experimentally measured IMEP distributions at 2000rpm.

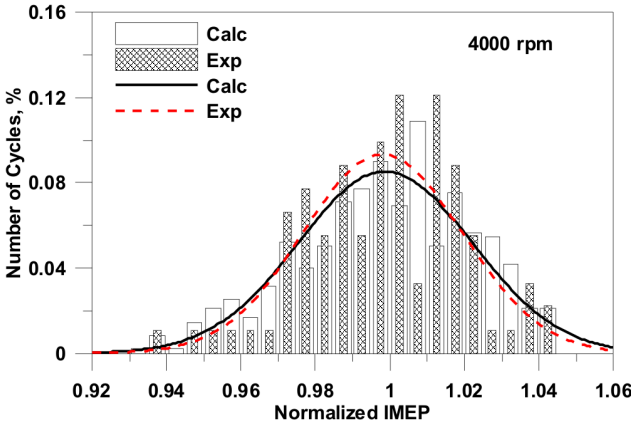

Figure 14: Computed and experimentally measured IMEP distributions at 4000rpm.

The described procedure allows computing a set of instantaneous pressure data statistically equivalent to the experimental one. This set only depends on a single parameter (x_{band}), well correlated to the COV values (Fig. 9).

Starting from this data set, a knock analysis is finally carried out on a cycle-by-cycle basis. Although the COV level does not determine any particular problem on the engine drivability, a moderate or even severe knocking may indeed arise in a number of individual cycles, depending on the local values of the previously listed P_i controlling parameters. Thermo-fluidynamic conditions occurring cycle-by-cycle in the unburned zone represent input data for the previously described knock model. This leads to the estimation of a statistical distribution of the computed knock indicators defined in Eqs. (3.2).

Figs. 15 and 16 show the cycle-by-cycle IMEP and Q_{ub} index variations in two different operating conditions. In both the cases, despite the low IMEP COV, a much higher variability level is found for the Q_{ub} index. This demonstrates that even small cycle-by-cycle differences may induce a dramatic effect on knocking occurrence, due

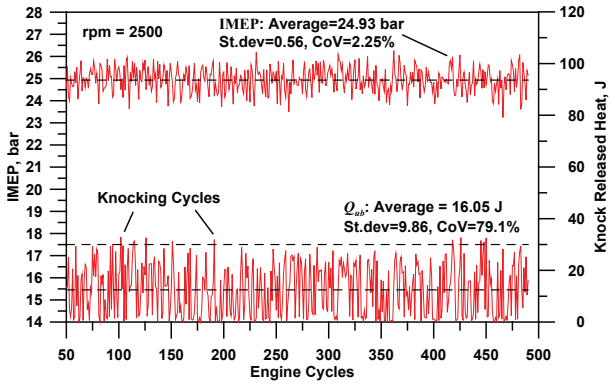

Figure 15: IMEP and Q_{ub} fluctuations at 2500rpm.

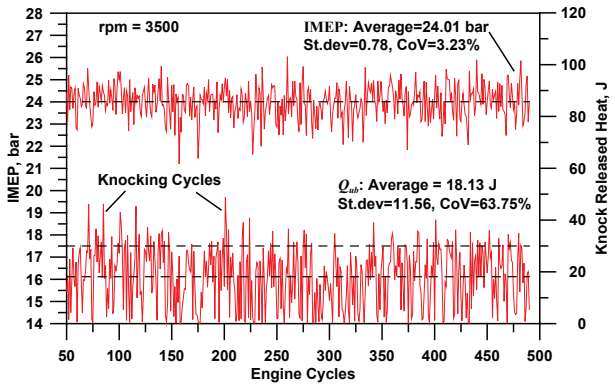

Figure 16: IMEP and Q_{ub} fluctuations at 3500rpm.

to the high non-linearity of the reactions rates involved in the knocking phenomenon. Moreover, once typical threshold limits are defined, (as an example Q_{ub}<20J no knocking, 20J <Q_{ub}<30J light knocking, Q_{ub}>30J knocking), Figs. 15 and 16 highlight that even if a knock-free operation is expected on the average cycle ($Q_{ub,av}$<20J), a certain percentage of individual cycles are characterized by a light or more severe knocking ($Q_{ub,i}$>30J). This behavior strongly depends on the selected spark advance. For this reason the developed procedure gives the possibility to specify the spark advance realizing only a prescribed and controlled percentage of individual knocking cycles.

In order to validate the results, the experimental estimation of a statistical distribution of the knock indicator is also required. Although, as said, the knock-limited spark advance is based on engine structural vibration measurements, the same signal cannot provide an adequate estimation of the CV of the knock intensity. The accelerometer signal, in fact, is characterized by a low signal-to-noise ratio, especially at high engine speeds, due to the presence of other knock-independent vibrations sources, like valve closing events and piston slap. Moreover, a local knock occurrence is considered as only induced by the presence of cyclic dispersion.

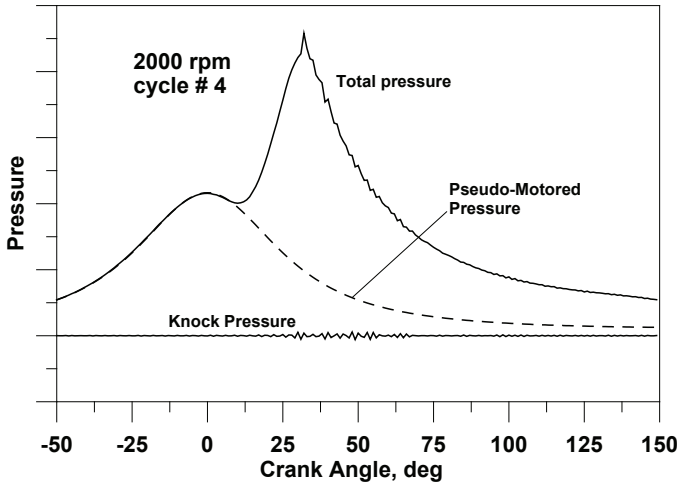

Figure 17: Total, pseudo-motored and knock pressures.

For this reason, the instantaneous pressure measurements are directly employed. The "knock-detection" technique utilizes a methodology originally proposed by Torregrosa et al. [15,16]. The procedure quantifies the radiated noise contribution coming from "resonance phenomena" in compression-ignition engines, due to the autoignition onset at the peripheral spray plume. Similarly, in a SI engine, the sudden knock-induced heat release determines small pressure pulsations at various resonant frequencies, which depend on the combustion chamber geometry and burned gas temperature. Being the axial dimension of the combustion chamber at the knocking onset usually lower than the radial one, the first circumferential resonant frequency is mainly related to the cylinder bore, and is typically greater than 4500Hz [17,18]. Basing on the above consideration, each single pressure cycle is band-pass filtered in a prescribed crank angle window (50° BTDC-150° ATDC), and a "knocking pressure" signal, p_{knock} is identified. Unfortunately, pressure data are acquired on a low resolution crank angle basis (1 CAD), which is just sufficient to capture at least the lowest frequency of the knocking phenomenon.

Fig. 17 highlights a single pressure cycle at 2000rpm characterized by a moderate knocking occurring at the pressure peak. A DFT based filtering process, applied in the 4500-6000Hz frequency range, allows to isolate the small amplitudes of the previously defined knocking pressure.

Knock intensity is then related to the resonance energy of the knocking pressure as:

$$E_{res} = \int_{-50}^{150} p_{knock}^2 d\vartheta, \tag{4.3}$$

and an experimental knock indicator I_2 is finally defined:

$$I_2 = \log_{10}\left[1.7e6\left(\frac{E_{res}}{E_{mot}}\right)\right]. \tag{4.4}$$

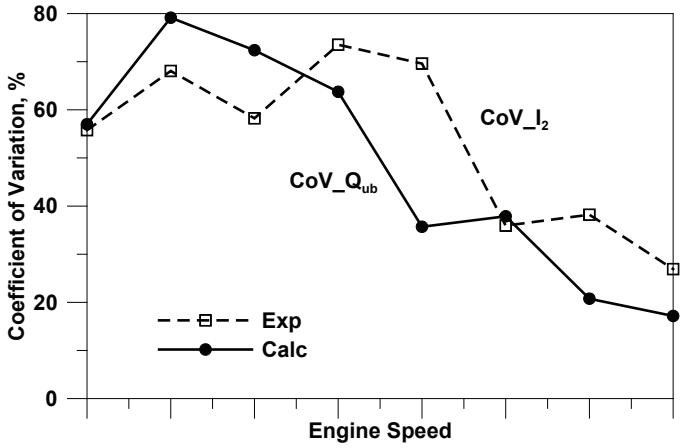

Figure 18: Coefficient of variation of the numerical (Q_{ub}) and experimental (I_2) knock indicators.

E_{mot} in Eq. (4.4) is a proper reference term computed as a function of a "pseudo-motored" pressure cycle, p_{mot}:

$$E_{mot} = \int_{-50}^{150} p_{mot}^2 d\vartheta, \qquad p_{mot}(\vartheta) = p_0 \Big(\frac{V_0}{V(\vartheta)} \Big)^{\gamma}. \tag{4.5}$$

V_0 being the volume at 50° CAD BTDC, p_0 the pressure of the "average" cycle at the same crank angle, and γ a suitable politropic exponent.

Eq. (4.4) roughly corresponds to other similar definitions of the knock index [18]. When applied to the whole set of 94 experimental pressure cycles, the described technique supplies the required statistical distribution of the knock indicators, to be compared with the experimental data.

Fig. 18 finally compares the coefficient of variation of the numerical (Q_{ub}) and experimental (I_2) knock indicators as a function of the engine speed. Although the quantitative agreement is not perfect, the trend seems to be correctly predicted. Both numerical and experimental values are very much higher than the IMEP COV levels. These results seem to validate the ones reported in Figs. 15 and 16 and confirm that even small cycle-by-cycle differences induce a dramatic effect on knocking occurrence. The knowledge of the computed profiles of Figs. 15, 16 and 18 could allow to perform, on a completely theoretical basis, a better choice of the spark advance, realizing, as said, only a prescribed and controlled percentage of individual knocking cycles.

5 Conclusions

The fluid-dynamic performance, the wall heat transfer, the combustion development and the knock risk of a "downsized" turbocharged spark-ignition engine are numerically estimated.

An accurate prediction of the combustion process and of the average in-cylinder pressure cycle are obtained, providing reliable initial conditions for the further modeling of the knocking phenomenon. The latter is realized through the solution of a reduced kinetic scheme within the unburned gas zone. Knock-limited spark advance is computed with good accuracy in the whole speed range of the investigated engine.

The model is extended to include the effects of the cyclic dispersion. The procedure allows to obtain a set of instantaneous pressure data statistically equivalent to the experimental one, depending on the assignment of a single parameter, well correlated to the COV values.

Finally, the relationship existing between the CV and the knock occurrence is highlighted and compared to an experimentally determined knock indicator. The reliability of this last parameter is limited by the low sampling frequency of the instantaneous pressure cycles, which only allows to identify the first knocking frequency. Additional experimental activities are required to further validate the procedure.

Despite the above limitations, the presented results demonstrate that even small cycle-by-cycle differences may induce a dramatic effect on knocking occurrence. This indicates the need to perform a better choice of the spark advance, accounting for the cyclic dispersion.

The numerical analysis puts into evidence a good potential to perform an optimal choice of the "knock-limited" spark advance on a completely theoretical basis.

References

[1] SAWAMOTO K., KAWAMURA Y., KITA T., AND MATSUSHITA K., *Individual cylinder knock control by detecting cylinder pressure*, SAE Paper 871911, 1987.

[2] LITAK G., KAMINSKI T., CZARNIGOWSKI J., GRZEGORZ A. K., AND WENDEKER G. M., *Combustion process in a spark ignition engine: analysis of cyclic peak pressure and peak pressure angle oscillations*, Meccanica., 44 (2009), pp. 1–11.

[3] GALLONI E., *Analyses about parameters that affect cyclic variation in a spark ignition engine*, Appl. Thermal. Eng., 29 (2009), pp. 1131–1137.

[4] HEYWOOD J. B., Internal Combustion Engine Fundamentals, McGraw-Hill Int. editions, 1988.

[5] BOZZA F., AND TORELLA E., *The employment of a 1D simulation model for the A/F ratio control in a VVT engine*, SAE Paper 2003-01-0027, also in SAE Transactions, J. Eng., 112 (2004), pp. 124–134.

[6] F. BOZZA, A. GIMELLI, D. SIANO, E. TORELLA, AND G. MASTRANGELO, *A quasi-dimensional three-zone model for performance and combustion noise evaluation of a twin-spark High-EGR engine*, SAE 2004 Transactions, J. Eng., 113 (2005), pp. 491–501.

[7] BOZZA F., GIMELLI A., MEROLA S. S., AND VAGLIECO B. M., *Validation of a fractal combustion model through flame imaging*, SAE 2005 Transactions, J. Eng., 114 (2006), pp. 973–987.

[8] POULOS S. G., AND HEYWOOD J. B., *The effect of chamber geometry on spark-ignition engine combustion*, SAE Paper 830334, 1983.

[9] BOZZA F., FONTANA G., GALLONI E., AND TORELLA E., *3D-1D analyses of the turbulent flow field, burning speed and knock occurrence in a turbocharged SI engine*, SAE Transactions, J. Eng., 116 (2008), pp. 1495–1507.
[10] GT-Power, User's Manual and Tutorial, GT-SUITE^{TM} Version 6.1, Gamma Technologies.
[11] HU H., AND KECK J., *Autoignition of adiabatically compressed combustible gas mixtures*, SAE Paper 872110, 1987.
[12] KECK J., AND HU H., *Explosions of adiabatically compressed gases in a constant volume bomb*, 21st International Symposium on Combustion, The Combustion Institute, 1986, pp. 521–529.
[13] TANAKA S., AYALA F., AND KECK J., *A reduced chemical kinetic model for HCCI combustion of primary reference fuels*, Combust. Flame., 132 (2003), pp. 219–239.
[14] AYALA F. A., AND HEYWOOD J. B., *Lean SI engines: the role of combustion variability in defining lean limits*, SAE Paper 2007-24-0030.
[15] TORREGROSA A. J., BROATCH A., MARTIN J., AND MONELLETTA L., *Combustion noise level assessment in direct injection diesel engines by means of in-cylinder pressure components*, Meas. Sci. Tech., 18 (2007), pp. 2131–2142.
[16] PAYRI F., BROATCH A., TORMOS B., AND MARANT V., *New methodology for in-cylinder pressure analysis in direct injection diesel engines-application to combustion noise*, Meas. Sci. Tech., 16 (2005), pp. 540–547.
[17] HUDSON C., GAO X., AND STONE R., *Knock measurement for fuel evaluation in spark ignition engines*, Fuel., 80 (2001), pp. 395–407.
[18] SAMIMY H., AND RIZZONI G., *Mechanical signature analysis using time-frequency signal processing: application to internal combustion engine knock detection*, Proceedings of the IEEE, 84(9) (1996), pp. 1330–1343.
[19] VERMOREL O., RICHARD S., COLIN O., ANGELBERGER C., BENKENIDA A., AND VEYNANTE D., *Towards the understanding of cyclic variability in a spark ignited engine using multi-cycle LES*, Combust. Flame., 156(8) (2009), pp. 1525–1541.